Int J Adv Manuf Technol (2017) 89:833–846
DOI 10.1007/s00170-016-9059-5

ORIGINAL ARTICLE

A cutting force predicting model in orthogonal machining of unidirectional CFRP for entire range of fiber orientation

Liangxi Chen[1] · **Kaifu Zhang**[1] · **Hui Cheng**[1] · **Zhenchao Qi**[1] · **Qingxun Meng**[1]

Received: 1 November 2015 / Accepted: 15 June 2016 / Published online: 12 July 2016

Abstract Cutting force prediction of orthogonal cutting unidirectional carbon fiber-reinforced plastic (UD-CFRP) is crucial in the reduction of machining defects. This paper aims to construct a force prediction model for orthogonal cutting of UD-CFRP using beams on elastic foundation theory and the minimum potential energy principle (MPEP) when fiber orientation (θ) varies from 0° to 180°. Models for different fiber orientation ranges were established separately, i.e., (1) $0°<\theta<90°$, (2) $90°\leq\theta<180°$, and (3) 0°. The deformation of the fibers was considered as a bending problem of a beam on elastic foundation. Total cutting force was composed of cutting forces from rake face, tool edge, and relief face of the cutting tool. As $0°<\theta<90°$, Vlazov's elastic foundation was introduced to calculate pressing forces between cutting tool edge and the representative volume element (RVE). The force applied on rake face was the integral value of resistant forces from those micro-elements of the curved chip based on well-established shear angle-cutting force relationships in Piispanen's card model. When $90°\leq\theta<180°$, non-uniform Winkler foundation was applied to calculate force between rake face and the RVE. When $\theta=0°$, the energy equation of the splitting process was constructed by using virtual crack close technique, and plugging force between rake face and the chip was derived from the equation. This mechanical model reveals mapping relationships between cutting forces and key variables such as the fiber orientation, rake angle, depth of cut, and so on. Corresponding experiments were conducted, and predictions were in acceptable agreement with the experimental measurements.

Keywords UD-CFRP · Beams on elastic foundation · Orthogonal cutting · Fiber orientation · Analytical model

Nomenclature

E_0	Transverse modulus of UD-CFRP
G	Young's modulus of elastic foundation
E_f	Young's modulus of fiber
G_m	Shear modulus of matrix
E_3	Effective modulus of the bouncing area
X_{fc}	Longitudinal compressive strength
X_{ft}	Longitudinal tensile strength of fiber
S_m	Matrix shear strength
U_f	Elastic strain energy of the fiber
U_m	Shear strain energy in the matrix
F_{xt}	Cutting force
F_{yt}	Thrust force
F_f	Friction force
μ	Friction coefficient
v	Poisson ratio of UD-CFRP
ζ	Shear strain of matrix
$2c$	Fiber spacing
r	Fiber radius
I_f	Second moment of area of the cross of fiber section of fiber
r_e	Tool edge radius
γ	Rake angle
α	Relief angle
θ	Fiber orientation
a_c	Depth of cut

✉ Kaifu Zhang
zhangkf@nwpu.edu.cn

[1] School of Mechatronics, Northwestern Polytechnical University, Mail Box 552, No. 127, Youyixi Road, Xi'an, Shaanxi 710072, China

t Thickness of laminate
H Thickness of elastic foundation

1 Introduction

Carbon fiber-reinforced plastic (CFRP), widely used in aerospace and military applications [1], offers a high strength-to-weight ratio, high modulus-to-weight ratio, and good dimensional stability. The post-fabrication operation, such as drilling [2, 3], milling [4, 5], and turning [6, 7], is basically a kind of cutting process and must ensure that the machined parts meet dimensional tolerance, surface quality, and other functional requirements [8]. However, cutting force is fiber orientation dependent because of the anisotropic properties of CFRP. During some drilling-like machining processes, the cutting edges, rotating around the center of the drill, cut unidirectional carbon fiber-reinforced plastic (UD-CFRP) of different fiber orientations at the same time. Also, unlike the metal chips that are formed from continuous shear plane mainly caused by the rake face of cutting tool, the material removal process of cutting CFRP is cyclic and is composed of different kinds of failure caused by rake face, relief face, and tool edge. So, the pull-out of the fibers, fiber-matrix debonding [9], and other manufacturing defects [10] are easy to occur as machining CFRP because of its inhomogeneity and anisotropy properties. The damages are considered caused by the use of improper cutting parameters, which always leads to the overlarge contacting forces (cutting forces) between cutting tool and workpiece. The overlarge cutting forces make the fibers and matrix break irregularly and accelerate tool wear. Prediction of cutting forces is of great importance to understand the cutting process and optimize cutting parameters and then defects can be reduced. Therefore, in order to get qualified CFRP components, there is a motivation for establishing a mechanical model of cutting UD-CFRP for entire range of fiber orientations.

For the purposes of reflecting material removal process, the orthogonal cutting configuration (OCC) was used in modeling. Lots of investigations about orthogonal cutting of fiber-reinforced plastics (FRPs) have been carried out. The experiment was conducted by Koplev et al. [11] who proposed that the fiber orientation had a crucial influence on chip formation of cutting FRPs, which has been validated by many following researches. Wang et al. [12, 13] conducted related experiments and found such phenomenon that there were three different mechanisms in orthogonal cutting unidirectional FRPs for entire fiber orientation (0–180°), i.e., (1) $0°<\theta<90°$, (2) $90°\leq\theta<180°$, and (3) 0°. The chip formation, when fiber orientation ranging from 0° to 90°, has been proposed that the broken chip surface was perpendicular to the fiber axis, and chip formation occurred through fracture along the fiber/matrix interface. Wang and Zhang [14, 15] conducted systematic experiments about orthogonal cutting of UD-CFRP and found the phenomenon of bouncing back. When the fiber orientation was less than 90°, three distinct deformation zones in cutting region, i.e., chipping, pressing, and bouncing, were first proposed.

In order to predict cutting forces in orthogonal cutting of unidirectional FRPs without expensive and time-consuming experiments, numerical simulation and analytical models have been used widely recently. Arola et al. [16, 17] used the macro-mechanical approach to analyze orthogonal cutting of unidirectional FRPs. A FE model based on conclusions of experimental research utilized a dual fracture criterion comprised of primary and secondary fracture, to describe the process of chip formation. The cutting force obtained by numerical simulations, when $0°<\theta<90°$, agreed well with experimental measurements, the thrust forces did not. A two-dimensional, two-phase macro-micro combined model with elastic fiber and elasto-plastic matrix was established by Rao et al. [18, 19]. Interaction between tool edge and materials with fiber orientation ranging from 0° to 90° was analyzed in detail. A combination of crushing and bending causes the failure of fiber, and the damage initiates from the fiber's front or back surface next to the tool edge. Cutting forces from the rake face and the flank face were not discussed in this research.

Obviously, FE simulations revealed the cutting mechanism and the process of materials failure visually. However, it did not establish a precise mathematical relationship between major cutting parameters and cutting forces. As a result, several analytical models for orthogonal cutting of unidirectional FRPs have been established. An analytical model was established by Bhatnagar et al. [20] who assumed that a crack propagation plane existed along fiber orientation at which the matrix sheared when fiber orientation is less than 90°, which is similar with Arola and Ramulu's conclusions [16]. The possibility proposed by them, three different models in the range of 0° to 180° fiber orientation, was confirmed by Wang's experimental conclusions [12]. Merchant's classical metal cutting model was applied to calculate cutting forces by assuming the shear plane angle as the fiber orientation where failure occurred. The model predicted accurately when $0°<\theta<90°$. Pwu and Hocheng [21] also established an analytical model as cutting perpendicular to the fiber axis by assuming the materials as a cantilever beam and being removed by bending in the cutting process. Based on the Wang and Zhang's [15] experimental investigation, Zhang et al. [22] developed a mechanical model to predict forces in orthogonal cutting UD-CFRP when $0°<\theta<90°$. The total cutting and thrust forces were the superimposed forces in the three deformation zones, which agreed well with experimental measurement. Cutting force in chipping region was calculated under the assumption of a theoretical shear plane, which was different from experimental observations of Bhatnagar et al. [20] and Arola and Ramulu [16]. A chip formation mechanism was proposed for fiber orientations larger than 90°; however, no model was developed.

All the researches mentioned above predicted cutting forces based on the assumption of a theoretical shear plane, as same as classical metal cutting models do. However, chip formation mechanism of cutting UD-CFRP is quite different from that of metal cutting; thus, it results in bigger predicting error to use the method and assumption of metal cutting model in developing UD-CFRP cutting model directly. Sahraie Jahromi and Bahr [23] avoided the shear plane assumption and proposed a microscopic mechanical model based on one improved cutting mechanisms suggested by Zhang et al. [22] to predict cutting forces when $90°\leq\theta<180°$. It was the first time that the representative volume element (RVE) has been taken out of CFRP and the deflection of the RVE has been analyzed by minimum potential energy principle (MPEP). Total cutting forces were the sum of forces applied on all the RVE within one chip, which simplified the interaction between the RVE and surrounding materials.

Beams on elastic foundation theory have already been used in modeling of composite strength [24, 25] and the buckling behavior of the sublaminate [26]. Considering supportive forces from surrounding materials, this paper applied beams on elastic foundation theory and the MPEP to construct mechanical model for entire range of fiber orientation, continuing the Qi et al. research [27]. The materials to be a chip were regarded as a beam structure, and surrounding materials behind were regarded as the elastic foundation. The deformation of fibers was considered as one bending problem of the beam on elastic foundation, and the beam's reflection was analyzed according to the MPEP. Models for different fiber orientation ranges were established separately, i.e., (1) $0°<\theta<90°$, (2) $90°\leq\theta<180°$, and (3) 0° [12, 16]. Finally, avoiding the assumption of a theoretical shear plane, one analytical model with the capability of calculating cutting forces for orthogonal cutting UD-CFRP under the entire range of fiber orientation was established.

2 Three different cutting mechanisms for entire range of fiber orientation

Fiber orientation, θ, measured clockwise from the machined surface. Mechanical models were constructed according to the observation of experiments. Within a range of fiber orientation from 0° to 180°, there exist three different mechanisms, i.e., (1) $0°<\theta<90°$, (2) $90°\leq\theta<180°$, and (3) 0°.

As shown in Fig. 1a, when $0°<\theta<90°$, three characteristic regions, i.e., region *A* (chipping), region *B* (pressing), and region *C* (bouncing), appear [16]. The chip formation process consists of two basic cutting mechanisms—bulking in perpendicular direction and sliding in parallel direction. With the progress of the cutting edge, fiber and matrix in region *B*, pressed by the tool edge, are bended and crushed [19]. In this case, the fiber is better supported by the material behind. Meanwhile, the fiber is easier to break under the tool edge with small deformation. After bulking of cutting materials, the blocky chip is pushed between rake face of cutting tool and supportive materials in region *A*. Finally, the force component along the chip axis makes chip slide out of the cutting zone. In region *C*, the bouncing back phenomenon occurs when a part of the material in the cutting path is pushed down during cutting but springs back partially elastically after the tool passes away.

When $\theta>90°$, as Fig. 1b, the tool exerts a different set of forces on the fiber, the tilting force perpendicular to the fiber axis is toward out of the cutting plane, and hence the fiber gets a weaker support from the surrounding materials. Thus, material tends to glide over the tool edge instead of being shorn off. The material in front of tool is bent until the resulted stress exceeds material strength and breaks often below the cutting plane.

In Fig. 1c, when $\theta=0°$, the most representative cutting phenomenon is a large split ahead of tool. Fracture initiates along the fiber axis causing a layer to peel and the tool advance causes the raising layer to act as a cantilever beam until it is broken under bending load. There also exists the phenomenon of bouncing back.

3 Modeling for different ranges of fiber orientation

The cutting forces along and perpendicular to the cutting direction are noted as the cutting and thrust forces, respectively. The positive directions of the forces are taken to be in the positive *x* and *y* directions. The fiber is considered elastic, and matrix is considered elasto-plastic [28]. Modeling is based on the following assumptions [25]:

1. Two-dimensional deformation
2. No shear in the fiber
3. No matrix extension or compression
4. Normal stress in the fiber that produces no mechanical work during the deformation of the fiber

A three-dimensional model may be more realistic; however, employing a circular cross section for fibers will increase the complexity of the equations obviously and weaken the mapping relationships between major cutting parameters and predictions of cutting forces. Therefore, two-dimensional deformation is assumed as mentioned before.

3.1 Pressing and pushing forces when $0°<\theta<90°$

In practical CFRP laminates, three neighboring fibers are rarely co-planar, and with the same spacing between neighbors, it does not agree with CFRP microstructure introduced in terms of RVE (Fig. 2). However, this non-uniformity will deteriorate

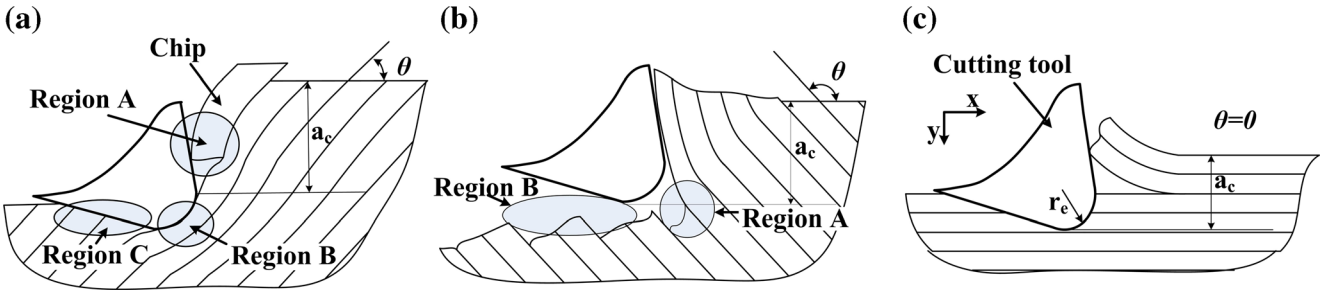

Fig. 1 **a–c** A schematic of the orthogonal cutting of UD-CFRP for different ranges of fiber orientation

the predicting accuracy of the matrix shear strain distribution and the predicting forces. Therefore, it is preferred to simplify the model if the more complex one will not significantly increase the accuracy [23]. The total cutting and thrust forces are the sum of forces from tool edge, rake face, and relief face.

3.1.1 Pressing force breaking the RVE (region B)

As shown in Fig. 3, the stresses along the RVE (Fig. 2) are typical of contact problems. The RVE is applied by uniform load q that is perpendicular to the fiber and friction force F_f which is parallel to the fiber, then a combination of crushing and bending causes the RVE failure. The total cutting and thrust forces should be taken from the minimum uniform load q that damages both fiber and matrix in the RVE. The length of the fiber is assumed to be relatively large compared to the thickness so that the beam theory is valid and the deformation of the RVE is considered as a bending problem of an infinite beam on elastic foundation as shown in Fig. 3. The fiber-matrix interaction within the supportive materials is ignored in this paper. The supportive materials are simplified as a two-parameter elastic foundation. Because if authors model the supportive materials considering effect of interactions, such as muti-beams model and elastic half-space model, the energy equation could not be solved in analytical model. Considering the UD-CFRP surrounding the RVE provides it with elastic support, which has obvious spreading ability of stresses, Vlazov's two-parameter elastic foundation was used in this mechanical model in order to improve the accuracy of the prediction. As shown in Fig. 3, the potential energy of the system is

$$\prod = \int_0^L \left[\frac{E_f I_f}{2} \left(\frac{d^2 y}{dx^2} \right)^2 + \frac{mG_m}{2} \left(\frac{dy}{dx} \right)^2 + \frac{Ey^2}{H(1-v_0^2)^2} + \frac{E^2 H}{24G(1+v_0^2)^2} \left(\frac{dy}{dx} \right)^2 \right] dx - qy|_{x=0} \tag{1}$$

Boundary conditions in this case are

$$\begin{aligned} &x \to \infty : y \to 0 \\ &x = o : \quad \frac{dy}{dx} = 0 \ , \quad \frac{d^3 y}{dx^3} = \frac{1}{EI} \frac{p}{2} \end{aligned} \tag{2}$$

According to principle of minimum potential energy, deflection of the beam can be written as

$$y = e^{-\lambda x} \left[\frac{p\lambda}{4E_f I_f (\lambda^3 + \lambda\beta^2)\beta} \sin\beta x + \frac{p}{4E_f I_f (\lambda^3 + \lambda\beta^2)} \cos\beta x \right] \tag{3}$$

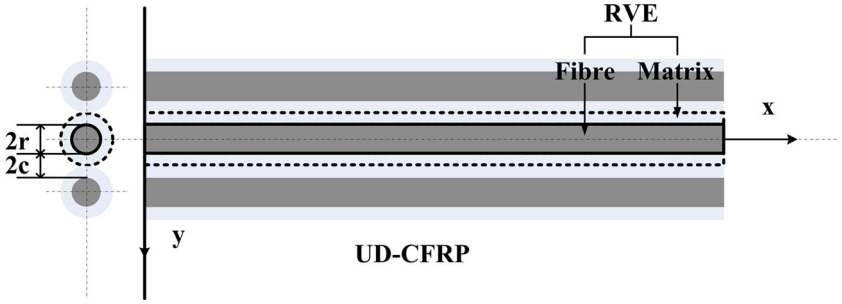

Fig. 2 Schematic of representative volume element (*RVE*) [25]

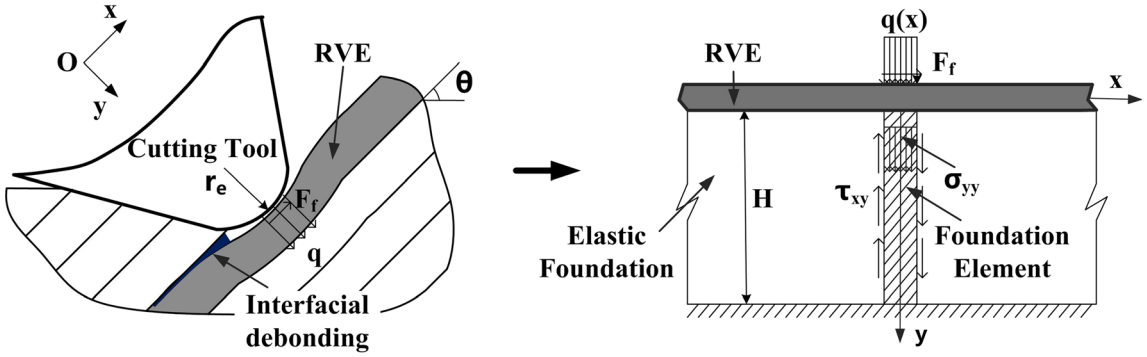

Fig. 3 The cutting and thrust force diagram in region *B* and corresponding sketch of model when $0° < \theta < 90°$

where

$$\lambda = \frac{1}{2}\sqrt{2\sqrt{\frac{2E}{H(1-v_0^2)^2 E_f I_f}} - \frac{mG_m}{E_f I_f} - \frac{EH}{12E_f I_f G(1+v_0^2)^2}}$$

$$\beta = \frac{1}{2}\sqrt{2\sqrt{\frac{2E}{H(1-v_0^2)^2 E_f I_f}} + \frac{mG_m}{E_f I_f} + \frac{EH}{12E_f I_f G(1+v_0^2)^2}}$$

According to the superposition principle, we get the deflection of the RVE by integrating y with respect to x, i.e.,

$$y_{total} = q\int_0^{\frac{L}{2}+x}\left\{e^{-\lambda\xi}\left[\frac{\lambda}{4E_f I_f(\lambda^3+\lambda\beta^2)\beta}\sin\beta\xi + \frac{1}{4E_f I_f(\lambda^3+\lambda\beta^2)}\cos\beta\xi\right]\right\}d\xi$$
$$+q\int_0^{\frac{L}{2}-x}\left\{e^{-\lambda\xi}\left[\frac{\lambda}{4E_f I_f(\lambda^3+\lambda\beta^2)\beta}\sin\beta\xi + \frac{1}{4E_f I_f(\lambda^3+\lambda\beta^2)}\cos\beta\xi\right]\right\}d\xi$$

Therefore, tensile stresses σ_f along the axis caused by frictional force are calculated as

$$\sigma_f = \frac{\mu\int_0^L q dx\cos\theta}{2r} \tag{4}$$

In cutting process, both fiber and matrix of the RVE should fail for a chip to form. Therefore, normal stress in fiber and shear stress in matrix should be calculated and compared to their strengths separately.

$$\sigma_x - \sigma_f - \mu_f(\sigma_y) = X_{ft} \tag{5}$$

The maximum stress along the fiber will occur at the front or rear surface where it contacts tool edge ($x = 0$). By Eq. (5), two different values of the uniform load q, which break the fiber, are obtained. The fiber fails if at any point the minimum requirement for the failure is met, so the smaller one, denoted as q_f, of the two q values determined should be chosen as the load that breaks the fiber.

Another failure mechanism is the excessive shear stress that results in matrix damage, and the maximum shear stress in matrix occurs at the location of $x = \pm\frac{L}{2}$ by $\frac{d^2 y_{total}}{dx^2} = 0$.

$$\tau_{max} = G_m \frac{dy}{dx}\Big|_{x=\frac{L}{2}} = S_m \tag{6}$$

The uniform load q damaging the matrix is obtained by solving the equation above and is denoted as q_m. Finally, the greater one between q_f and q_m is the actual uniform load that cutting edge applies on RVE in cutting process.

3.1.2 Pushing force leading to chip sliding (region A)

Loaded by component of pushing force being perpendicular to chip's axis, the chip, considered as a beam structure, is bent and slides along the cure of deflection. In order to get the value of pushing force, the angle of sliding path of every micro-part of the chip is calculated based on the chip's deflection firstly, and then all the pushing forces loading on micro-part of the chip can be solved by well-established shear angle-cutting force relationships in Piispanen's card model.

In Fig. 4, the force R, which the tool exerts on the chip, can be divided into two components denoted N and F'. Force N works normal to the face of the tool. Force F', a friction force,

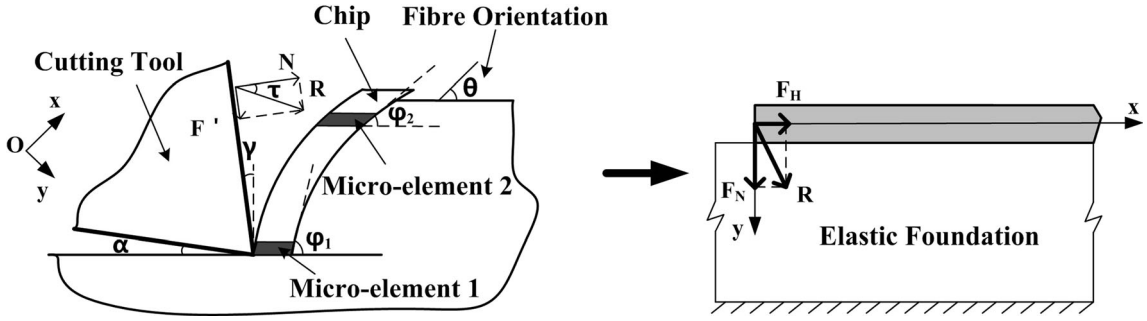

Fig. 4 The cutting and thrust force diagram in region *A* and corresponding sketch of model when $0° < \theta < 90°$

works counter to sliding of the chip. As a reaction to force *R*, the forces applied on the chip by surrounding materials can also be divided into two components, F_n and F_s, the former affects perpendicular to fiber axis and provides the chip with elastic support. The other component acts along the chip's axis and resists the removal of the chip. The deformation of the chip is considered as a bending problem of a semi-infinite beam on elastic foundation as shown in Fig. 4. Deflection of the beam can be calculated by

$$y = \frac{F_N}{2EI\beta^3} e^{-\beta x} \cos\beta x \tag{7}$$

The chip is divided into micro-elements along its axis, which is shown in Fig. 4. Therefore, every specific micro-element slides along a certain direction which can be calculated by deflection of the chip

$$\phi = \theta + \arctan\left(\frac{F_N}{2EI\beta^3} e^{-\beta x}(\cos\beta x + \sin\beta x)\right) \tag{8}$$

Force dF_N between every micro-element and rake face of the cutting tool can be calculated based on well-established shear angle-cutting force relationships in Piispanen's card model, i.e., [29]

$$dF_N = F_s \tan(\phi + \tau - \gamma) dx \tag{9}$$

Substituting Eq. (8) into Eq. (9) and doing integrals of both sides of the equation,

$$\frac{F_N - \frac{1}{a_2}L}{(b_2 - a_2 c_2)\left(-\frac{1}{2c_2\beta}\right)} = \ln\left\{\frac{\left[1 + F_N c_2 e^{-\beta L}(\cos\beta L + \sin\beta L)\right]\left[1 + F_N c_2 e^{-\beta L}(\cos\beta L + \sin\beta L)\right]}{(1 + F_N c_2)^2}\right\} \tag{10}$$

Where

$$a_2 = F_s \tan(\theta + \tau - \gamma) \;,\; b_2 = \frac{F_s}{2EI\beta^2} \;,\; c_2 = -\frac{\tan(\theta + \tau - \gamma)}{2EI\beta^2}$$

The value of F_N is calculated by computer, and then the cutting and thrust forces on the rake face of the cutting tool are expressed as

$$\begin{cases} F_{xp} = \dfrac{F_N}{\sin(\theta + \tau - \gamma)} \cos(\gamma - \alpha) \\ F_{yp} = -\dfrac{F_N}{\sin(\theta + \tau - \gamma)} \sin(\gamma - \alpha) \end{cases} \tag{11}$$

3.1.3 Total cutting and thrust forces

The contact forces between relief face of cutting tool and the bouncing back materials (region *C*) have already been calculated by Zhang et al. [22], which are decomposed into *x* and *y* directions denoted by F_{yb} and F_{xb},

$$\begin{cases} F_{xb} = \dfrac{1}{2} r_e E_b t \cos^2\alpha \\ F_{yb} = \dfrac{1}{2} r_e E_b t (1 - \mu\cos\alpha\sin\alpha) \end{cases} \tag{12}$$

Adding forces in region *A*, region *B*, and region *C* and decomposing it into *x* and *y* directions, we get the cutting and thrust forces as

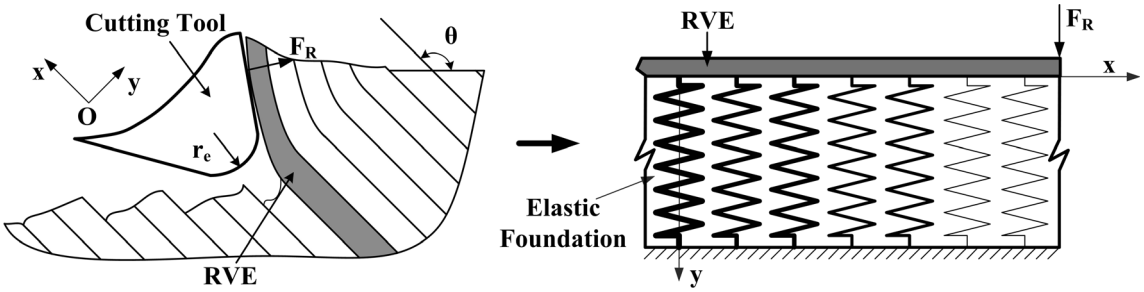

Fig. 5 The cutting and thrust force diagram and corresponding sketch of model when $90° \le \theta < 180°$

$$\left.\begin{aligned} F_{xt} &= \int_0^L q_{max} dx \sin\theta + F_f \cos\theta + F_{xp} + F_{xb} \\ F_{yt} &= \int_0^L q_{max} dx \cos\theta + F_f \sin\theta + F_{yp} + F_{yb} \end{aligned}\right\} \quad (13)$$

3.2 Bending force when $90° \le \theta < 180°$

As shown in Fig. 5, materials surrounding the RVE support the RVE in a special way. Toward the surface of workpiece, supportive effect becomes weaker. There are no surrounding materials supporting the RVE near the surface. Therefore, the bending force that breaks the RVE is calculated as follows: (1) the deflection of the RVE is calculated by MPEP; (2) the point where the maximum normal stress occurs is ensured according to the deflection; and (3) calculating the minimum bending force as the maximum normal stress reaches the flexural strength of the fiber.

The deformation of the RVE can be considered as a bending problem of a semi-infinite beam on non-uniform Winkler foundation [30], as shown in Fig. 5. Coefficient of foundation k changes in a linear fashion along x direction at the range $0 < x \le L$ and $k = 0$ at $x = L$ and $k = k_0$ at $x \le 0$. We can express it as

$$k = k_0 \tan(\theta)\left(1 - \frac{x}{L}\right) \quad (14)$$

k_0 is the coefficient of uniform Winkler foundation [30]. Value of L can be determined by experiment. The potential energy of bending RVE is

$$\begin{aligned} \prod &= U - \sum w \\ &= \int_0^L \left[\frac{E_f I_f}{2}\left(\frac{d^2y}{dx^2}\right)^2 + \frac{mG_m}{2}\left(\frac{dy}{dx}\right)^2 + \frac{1}{2}ky^2\right] dx - Fy|_{x=L} \end{aligned} \quad (15)$$

Using Ritz method, the approximate deflection of a beam with two degree of freedom is written as

$$y = a_1 x^2 + a_2 x^3 \quad (16)$$

According to the principle of minimum potential energy, the coefficients can be obtained

$$\left\{\begin{aligned} a_1 &= \frac{B - CL}{AB - C^2} F_R L^2 \\ a_2 &= \frac{AL - C}{AB - C^2} F_R L^2 \end{aligned}\right. \quad (17)$$

Where

$$\begin{aligned} A &= 4E_f I_f L + \frac{4}{3} m G_m L^3 + \frac{1}{30} k_0 \tan\theta L^5 \\ B &= 12E_f I_f L^3 + \frac{9}{5} m G_m L^5 + \frac{1}{56} k_0 \tan\theta L^7 \\ C &= 6E_f I_f L^2 + \frac{3}{2} m G_m L^4 + \frac{1}{42} k_0 \tan\theta L^6 \end{aligned}$$

Matrix in cutting region has already been damaged before fiber breakage, and fiber of the RVE breaks at the point where maximum normal stress exceeds the flexural strength of fiber, where curvature of deflection K reaches a maximum. The value of K is

$$K = \frac{|2a_1 + 6a_2 x|}{\left(1 + (2a_1 x + 3a_2 x^2)^2\right)^{\frac{3}{2}}} \quad (18)$$

$\frac{dK}{dx} = 0$ when K reaches a maximum, then the x coordinate x_0, where fiber breaks, is obtained

$$x_0 = \frac{1}{30a_2^2}\left\{-10a_1 a_2 + 2\left[10a_1^2 a_2^2 + 15a_2^2\left(a_1^4 + 5a_2^2\right)^{\frac{1}{2}}\right]^{\frac{1}{2}}\right\} \quad (19)$$

Substituting Eq. (19) into Eq. (20), the maximum value of curvature of deflection K_{max} is obtained. Hence, the total cutting force F_R, which is needed to break the fiber, is calculated by substituting K_{max} into $\sigma_{max}^{bend} = E_f r K_{max}$. Total forces when $90° \le \theta < 180°$ are

$$\left.\begin{aligned} F_{xt} &= F_R \cos\gamma \\ F_{yt} &= -F_R \sin\gamma \end{aligned}\right\} \quad (20)$$

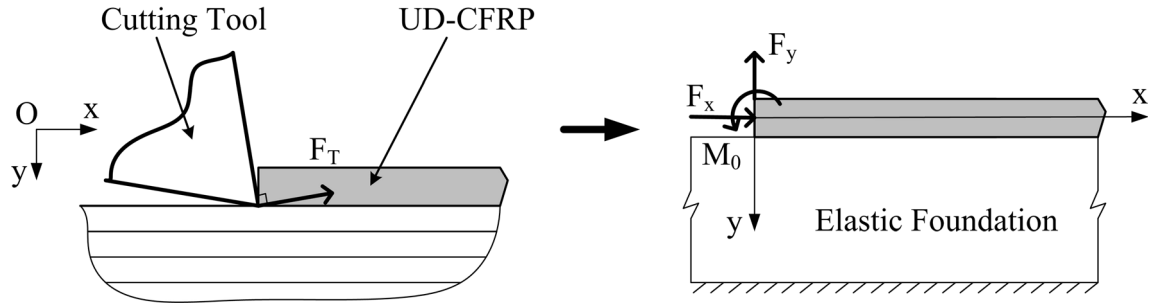

Fig. 6 The cutting and thrust force diagram on rake face and corresponding sketch of model when $\theta = 0°$

3.3 Plugging forces as splitting when $\theta = 0°$

As the chip is built up by the split failure, the deformation of the part to be a chip before the split occurrence is considered as a bending problem of a semi-infinite beam on elastic foundation as shown above. As the split extension is extremely rapid, cutting forces do no work [31] and the cutting and thrust forces that lead to split occurrence can be calculated by constructing an energy equation of the process of splitting, i.e., energy stored in the whole system before split occurrence U_{I} can be added by the releasing strain energy U_{II} during splitting and the remaining strain energy of the separated chip U_{III},

$$U_{\mathrm{I}} = U_{\mathrm{II}} + U_{\mathrm{III}} \tag{21}$$

3.3.1 Total strain energy before split occurrence

Before splitting, as shown in Fig. 6, the part to be a chip is pushed by a cutting tool, which can be considered the beam acted upon by forces parallel and perpendicular to fiber axis (F_x, F_y) and torque (M_0) at the end. In order to get the value of the system's energy before split occurrence, deflection of the beam could be figured out by MPEP.

The potential energy of the system before split occurrence is the sum of the potential energies due to the bending of the beam and the deformation of the elastic foundation minus the work done by the applied load at the end, which can be written as

$$\begin{aligned} \Pi_{\mathrm{F}} = {} & \frac{t}{4r+4c}\int_0^{+\infty} E_{\mathrm{f}} I_{\mathrm{f}} \left(\frac{d^2y}{dx^2}\right)^2 + mG_{\mathrm{m}}\left(\frac{dy}{dx}\right)^2 dx \\ & + \frac{1}{2}\int_0^{+\infty} ky^2 dx - \frac{F_x}{2}\int_0^{+\infty}\left(\frac{dy}{dx}\right)^2 dx + F_y y|_{x=0} \\ & + \frac{1}{2}F_x t\left.\frac{dy}{dx}\right|_{x=0} \end{aligned} \tag{22}$$

Where

$$m = A_{\mathrm{m}}\left(\frac{c+r}{r}\right)^2 = \pi(c+r)^2\left(\frac{1-\mathrm{vol_f}}{\mathrm{vol_f}}\right)$$

The principle of minimum potential energy

$$\frac{d^4y}{dx^4} + A\frac{d^2y}{dx^2} + B = 0 \tag{23}$$

Where

$$A = \frac{F_{\mathrm{x}} - \dfrac{t}{2r+2c}mG_{\mathrm{m}}}{\dfrac{t}{2r+2c}E_{\mathrm{f}}I_{\mathrm{f}}} \quad , \quad B = \frac{k}{\dfrac{t}{2r+2c}E_{\mathrm{f}}I_{\mathrm{f}}}$$

The boundary conditions in this case are written as

$$\begin{aligned} & x \to \infty : \quad y = 0 \\ & x = 0 \quad : \quad EI\frac{d^2y}{dx^2} = \frac{1}{2}F_{\mathrm{x}}t \quad , EI\frac{d^3y}{dx^3} = F_{\mathrm{y}} \end{aligned} \tag{24}$$

Deflection of the beam is

$$y = e^{-\lambda x}(a_1\cos\beta x + b_1\sin\beta x) \tag{25}$$

Where

$$\lambda = \sqrt{2\sqrt{B} - A} \quad , \quad \beta = \sqrt{2\sqrt{B} + A}$$

$$a_1 = \frac{\left(\lambda^3 - 3\lambda\beta^2\right)\dfrac{1}{2}t + \left(\lambda^2 - \beta^2\right)\tan(\alpha)}{EI\beta\left(\lambda^2+\beta^2\right)^2} \quad , \quad b_1 = \frac{\left(3\lambda^3 - \beta^2\right)\dfrac{1}{2}t + 2\lambda\tan(\alpha)}{EI\beta\left(\lambda^2+\beta^2\right)^2}$$

The value of the system's energy before split occurrence can be calculated according to the beam deflection, which is composed of strain energy in fiber ($U_{\mathrm{bending,fiber}}$), matrix ($U_{\mathrm{bending,matrix}}$), and elastic foundation (U_{spring}), it is written as

$$U_{\mathrm{I}} = U_{\mathrm{bending,fiber}} + U_{\mathrm{bending,matrix}} + U_{\mathrm{spring}} \tag{26}$$

Equations of every part's energy above express similarly as each other, so, U_{I} is

$$U_{\mathrm{I}}=\sum_{i=1}^{3}A_i\left[\frac{1}{4\lambda}\left(B_i^2+C_i^2\right)+\frac{\lambda}{4\left(\lambda^2+\beta^2\right)}\left(C_i^2-B_i^2\right)+\frac{\beta}{2\lambda^2+2\beta^2}B_iC_i\right]F_x^2 \tag{27}$$

where

$$A_1=\frac{tE_{\mathrm{f}}I_{\mathrm{f}}}{4r+4c}\quad,\quad B_1=2a\lambda\beta+b\lambda^2-b\beta^2\quad,\quad C_1=a\lambda^2-a\beta^2$$
$$A_2=\frac{tmG_{\mathrm{m}}}{4r+4c}\quad,\quad B_2=b\lambda-a\beta\quad,\quad C_2=b\lambda-a\beta$$
$$A_3=\frac{k}{2}\quad,\quad B_3=b\quad,\quad C_3=a$$

3.3.2 Releasing energy as splitting

The end of the beam is loaded by F_x and F_y, so the deformation of the split failure is classified into an opening mode and an edge sliding mode [32]. The value of releasing strain energy can be calculated using virtual crack close technique, as

$$U_{\mathrm{II}}=\frac{1}{2}\int_0^L\left(\sigma_y v+\tau_{xy}u\right)dx \tag{28}$$

The stresses σ_y, σ_y on the split line (x axis) before the split extension and the displacements v, u after the split extension are obtained from equations of stress and displacement in mode I and model II, respectively, which is described as

$$U_{\mathrm{II}}=\frac{L}{\pi E}\left[K_{\mathrm{I}}(a_0)K_{\mathrm{I}}(a_0+L)+K_{\mathrm{II}}(a_0)K_{\mathrm{II}}(a_0+L)\right] \tag{29}$$

where K_{I}, K_{II} are the stress intensity factors.

3.3.3 Remaining strain energy of the chip after splitting

The chip buckles and moves apart from the cutting area in the state of the split length (a_0+L), where a_0 is length of initial crack and L is the split length, which has already become a cantilever. The end of cantilever is loaded by F_{xm} which is parallel to fiber axis and F_{ym} which is perpendicular to fiber axis.

$$F_{\mathrm{xm}}=\frac{\pi^2\mathrm{EI}}{4(a_0+L)^2} \tag{30}$$

The split extension is so rapid that the cutting tool's displacement during this process is negligible to be ignored. The deflection of the beam on elastic foundation at the instant of the split occurrence, $y|_{x=0}$, is equal to the maximum deflection of a cantilever. In such circumstance, torque caused by F_{xm} is negligible to be ignored.

$$y|_{x=0}=\frac{F_{\mathrm{ym}}(a_0+L)^3}{3\mathrm{EI}} \tag{31}$$

Combining Eq. (30) and Eq. (31)

$$a_0+L=\frac{12e}{\pi^2}F_x \tag{32}$$

$$\begin{cases}F_{\mathrm{xm}}=\dfrac{\pi^6\mathrm{EI}}{576e^2}\dfrac{1}{F_x^2}\\ F_{\mathrm{ym}}=\dfrac{\pi^6\mathrm{EI}\tan(\alpha)}{576e^2}\dfrac{1}{F_x^2}\end{cases} \tag{33}$$

where

$$a_0=\frac{y|_{x=0}}{\cos x}\quad,\quad e=\frac{\left(\lambda^3-3\lambda\beta^2\right)\frac{1}{2}t+\left(\lambda^2-\beta^2\right)\tan(\alpha)}{\mathrm{EI}\beta\left(\lambda^2+\beta^2\right)^2} \tag{34}$$

Substituting Eqs. (30) and (34)into (29)

$$U_{\mathrm{II}}=\frac{(12\cos(\alpha)-\pi^2)(1+\tan(\alpha)\pi^2 I)}{2304\sqrt{3\cos(\alpha)}e^2}\frac{1}{F_x} \tag{35}$$

Total strain energy of bending cantilever is

$$U_{\mathrm{III}}=\frac{1}{2}\int_0^{a_0+L}F_{\mathrm{ym}}(y|_{x=0})dx \tag{36}$$

3.3.4 Total forces resulting in splitting

Combining Eqs. (21), (27), (35), and (36), which is

$$W_1F_x^3-W_2F_x-W_3=0 \tag{37}$$

Where

$$W_1=\sum_{i=1}^{3}A_i\left[\frac{1}{4\lambda}\left(B_i^2+C_i^2\right)+\frac{\lambda}{4\left(\lambda^2+\beta^2\right)}\left(C_i^2-B_i^2\right)+\frac{\beta}{2\lambda^2+2\beta^2}B_iC_i\right]$$
$$W_2=\frac{\mathrm{EI}\tan^2\alpha}{96}\quad,\quad W_3=\frac{(12\cos(\alpha)-\pi^2)(1+\tan(\alpha)\pi^2 I)}{2304\sqrt{3\cos(\alpha)}e^2}$$

Therefore,

$$\begin{cases}F_x=\left(\dfrac{1}{6W_1}+2W_2\right)M\\ F_y=\left(\dfrac{1}{6W_1}+2W_2\right)M\tan(\alpha)\end{cases} \tag{38}$$

where

$$M=\frac{1}{\sqrt[3]{\left[108W_3+12\sqrt{3}\sqrt{\dfrac{27W_1W_3^2-4W_2^3}{W_1}}\right]W_1^2}}$$

3.3.5 Total cutting and thrust forces

The bouncing back force in region C has already been calculated in Eq. (12), and total force was decomposed into x and y directions which are called cutting and thrust forces denoted by F_{yb} and F_{xb}, i.e.,

$$\left.\begin{aligned} F_{xt} &= F_x - F_{xb} \\ F_{yt} &= F_x \tan(\alpha) + F_{yb} \end{aligned}\right\} \tag{39}$$

4 Experiment and analysis

4.1 Experimental setup

A series of experiments were performed to measure the cutting and thrust forces. The experiments were carried on a XKN713 numerical control machining center. The spindle was fixed in order to do orthogonal cutting when cutting tool along the x coordinate axis. The workpiece was fixed to the fixture which is mounted on the dynamometer. The experimental devices and workpiece are shown in Fig. 7. The forces were measured by a Kistler 9257A quartz three-component platform dynamometer and Kistler 5073 charge amplifier. The data was processed on a HVM GEN2i data recorder.

The customized carbide tool was designed for orthogonal cutting with different rake angles. A unidirectional carbon plain weave fabric/epoxy resin (T300/Epoxy) composite plate was manufactured into a series of rectangle plates with different fiber orientations. The thickness per layer is 0.25 mm and then the total thickness, i.e., width of cut, is 3.75 mm. The specific material properties are given in Table 1.

Several groups of experiments have been conducted by controlling different variables, such as fiber orientations ($\theta = 0°$, 15°, 30°, 45°, 60°, 75°, 105°, 135°, 150°, 165°), rake angle (5°, 15°, 25°), and cutting depth (0.10, 0.15, 0.20 mm). Feed rate was kept at the machine maximum feed of 1 m/min for all of the experiments. Each experiment with a group of special parameters was repeated three times in order to minimize the random error. Figure 7c shows the experimental real-time forces recorded by dynamometer for $\gamma = 15°$ and $a_c = 0.1$ mm when $\theta = 60°$ and $\theta = 135°$.

Compared with cutting metal materials, the measured cutting and thrust forces fluctuate more fiercely especially when $90° \le \theta < 180°$. However, forces are actually varying in a certain range; therefore, we choose the mathematical expectation of the forces of steady state in x and y directions as the experimental cutting and thrust forces.

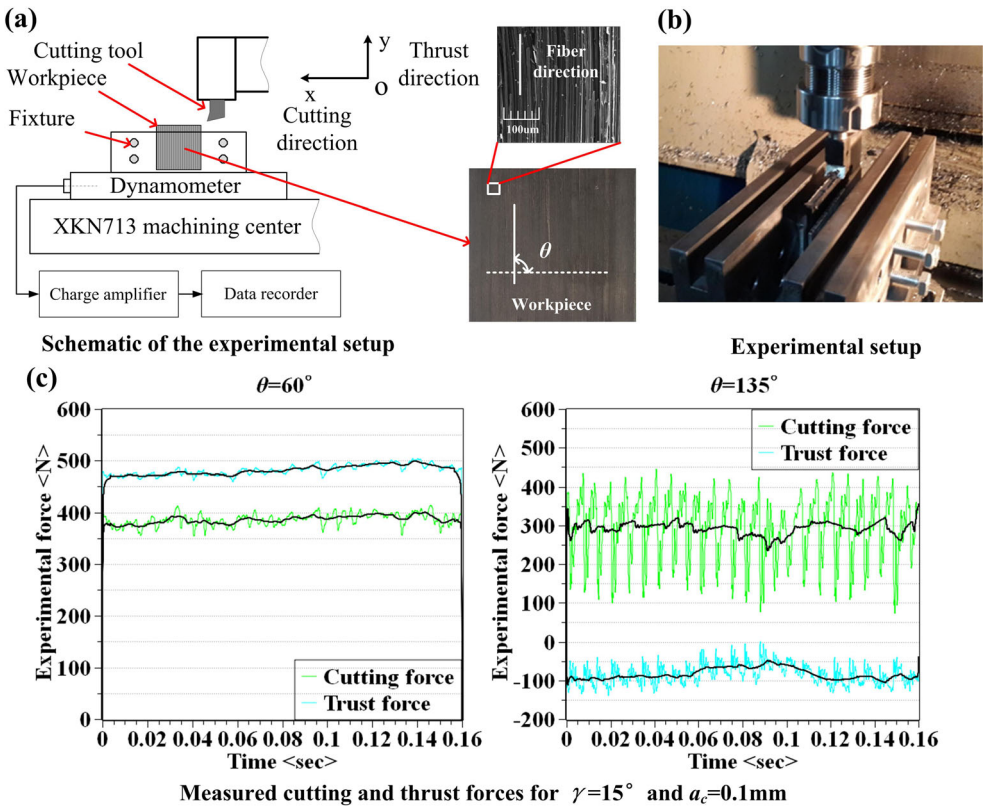

Fig. 7 Experimental setup and measurements. **a** Experimental setup. **b** Schematic of the experimental setup. **c** Measured cutting and thrust forces for $\gamma = 15°$ and $a_c = 0.1$ mm when $\theta = 60°$ and $\theta = 135°$

Table 1 List of material properties T300/Epoxy

Fiber radius (r)	3.5 μm	Fiber spacing ($2c$)	4.7 μm
Passion ratio (v)	0.4	Friction coefficient (μ)	0.15
Young's modulus of the fiber (E_f)	230 GPa	Shear modulus of the matrix (G_m)	1.48 GPa
Fiber tensile strength (X_{ft})	2.50 GPa	Fiber compressive strength (X_{fc})	2.00 GPa
Matrix shear strength (S_m)	70 MPa	Young's modulus of the bouncing back area (E_3) [22]	5.5 GPa

4.2 Comparison between analytical and experimental results

Figures 8, 9, and 10 demonstrate the variation of the forces with the fiber orientation, rake angle, and depth of cut, and it is described in detail below.

Fiber orientation greatly influenced the cutting forces as shown above. As $0° \le \theta < 90°$, cutting forces decrease and then increase as θ increases (Fig. 8). The minimum value of cutting forces appears when θ ranges from 20° to 30°, and the specific value of θ depends on a special variable combination, i.e., rake angle and depth of cut. The thrust force increases and then decreases with the increase of the fiber orientation. When $90° \le \theta < 180°$, as shown in Fig. 9, cutting and thrust forces decrease as θ increases, thrust force is negative because materials applied a pulling force to the tool.

As shown in Figs. 8a, b, 9a, b, and 10a, the depth of cut also influences cutting and thrust forces remarkably. It proves that forces applied on rake face of the cutting tool occupy an important proportion of the total cutting forces.

The effect of rake angle is not so significant as compared with the influence of the other two variables. In the general case, cutting and thrust forces are smaller for bigger rake angle for entire range of fiber orientations, as shown in Figs. 8c, d, 9c, d, and 10b. An interesting phenomenon is that the thrust force for $\gamma = 25°$ is larger than that of $\gamma = 15°$ when $0° \le \theta < 90°$, as shown in Fig. 8d, and it has been proved by both model prediction and experiment. This phenomenon is related to the

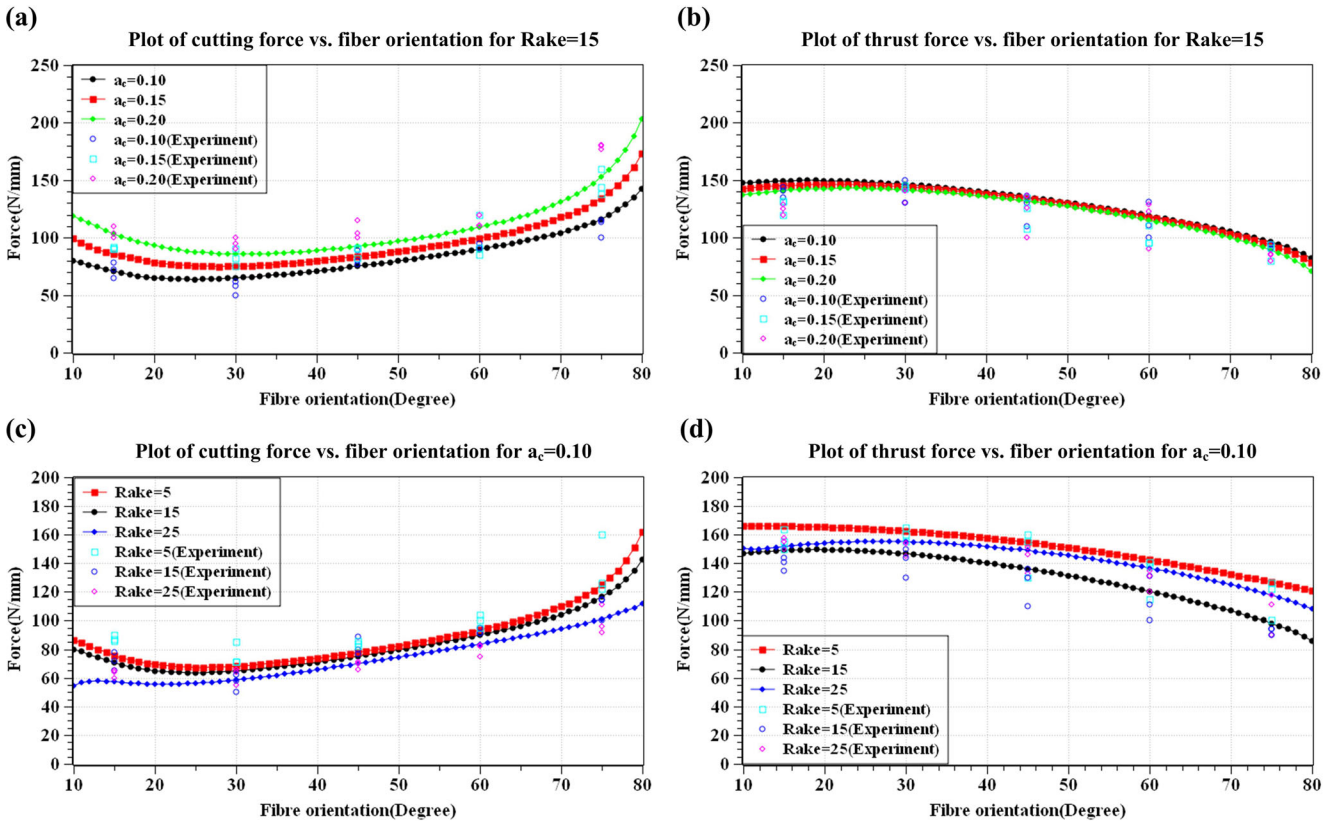

Fig. 8 Comparison between model predictions and experimental measurements when depth of cut and rake angle change ($0° < \theta < 90°$). **a** Plot of cutting force vs. fiber orientation for rake = 15. **b** Plot of thrust force vs. fiber orientation for rake = 15. **c** Plot of cutting force vs. fiber orientation for $a_c = 0.10$. **d** Plot of thrust force vs. fiber orientation for $a_c = 0.10$

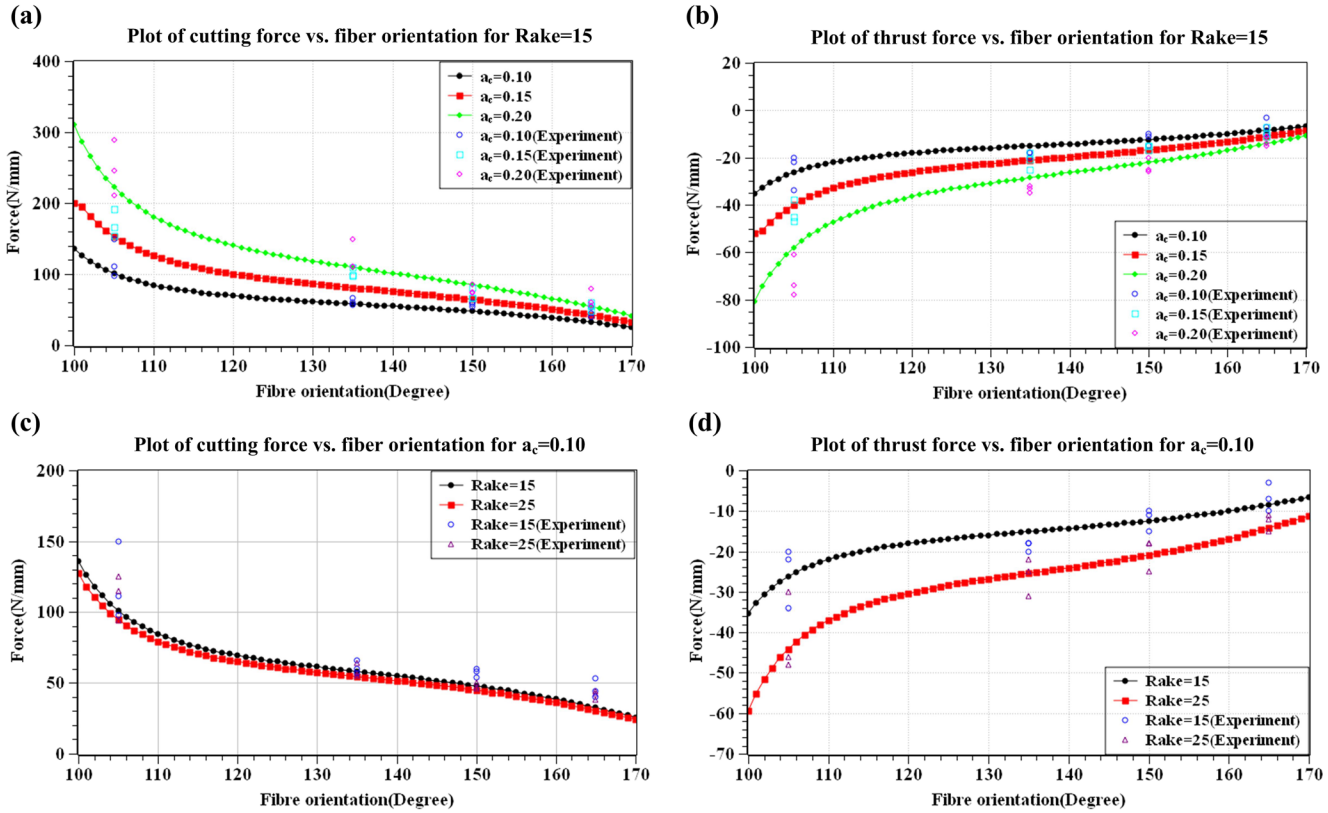

Fig. 9 Comparison between model predictions and experimental measurements when depth of cut and rake angle change ($90° \le \theta < 180°$). **a** Plot of cutting force vs. fiber orientation for rake = 15. **b** Plot of thrust force vs. fiber orientation for rake = 15. **c** Plot of cutting force vs. fiber orientation for $a_c = 0.10$. **d** Plot of thrust force vs. fiber orientation for $a_c = 0.10$

variation of the direction and magnitude of forces applied on rake face.

The model predictions and the experimental measurements are compared and agree well with each other. The results show that the average absolute value of relative errors between predictive and measured values of cutting and thrust forces is 17 and 22 %, respectively, which is in a reasonable range [23]. Variance between the predicted and experimental result is due to following reasons:

1. According to the experimental observation, there exists delamination near the surface of the specimen after the cutting tool passed through. So, some fibers are not broken because of stiffness reduction. Such phenomenon was more obvious when $90° \le \theta < 180°$; therefore, it led to an error.
2. Forces are predicted using macro-mechanical properties of the UD-CFRP. However, in small deformation zone, the strength of the materials will be higher since the probability and number of defects will be less [33].

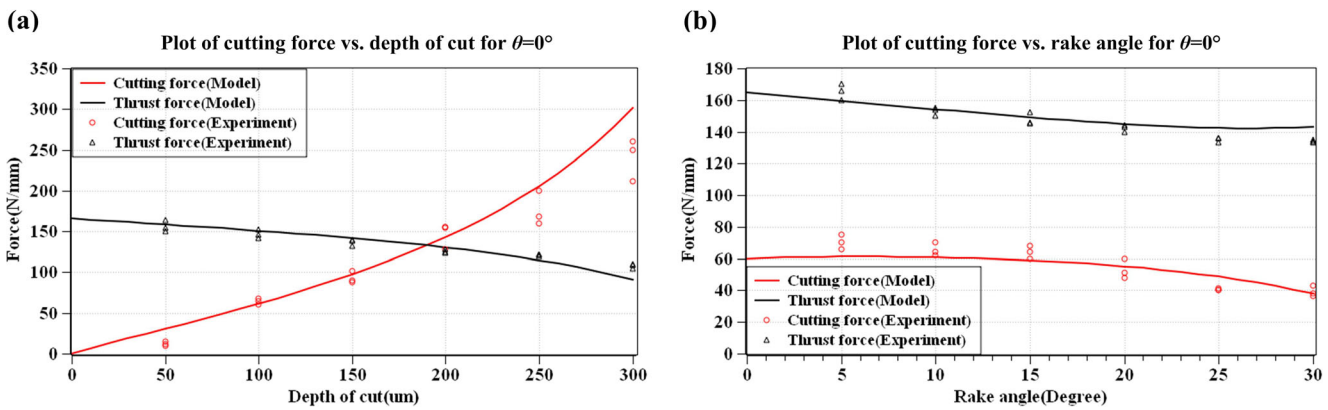

Fig. 10 Comparison between model predictions and experimental measurements when rake angle and depth of cut change ($\theta = 0°$). **a** Plot of cutting force vs. depth of cut for $\theta = 0°$. **b** Plot of cutting force vs. rake angle for $\theta = 0°$

3. Assumptions and boundary conditions cannot match real cutting situation perfectly.

Within some particular ranges of fiber orientation, such as $0°<\theta<10°$, $170°<\theta<180°$, and $80°<\theta<100°$, there exist several different cutting mechanisms that mix up and influence with each other. The modeling with fiber orientation in these ranges will be discussed in a separate paper by using the weighted algorithms.

5 Conclusion

From the energy point of view, this paper initially constructed a theoretical model for predicting cutting and thrust forces in orthogonal cutting of UD-CFRP under the entire range of fiber orientation based on beams on elastic foundation theory and the principle of minimum potential energy.

1. The specific relationship between cutting parameters, such as fiber orientation, depth of cut, rake angle, and cutting and thrust forces, has been expressed accurately. It was found that fiber orientation has the most significant influence on cutting and thrust forces, depth of cut does less, and rake angle does the least.
2. Corresponding experiments with a group of special parameters have been conducted, and model predictions agree well with the experimental measurements.
3. This model has formed the foundation for process parameters optimization, tool performance improvement, and cutting cost reduction. It could also be used to predict forces in other manufacturing processes of CFRP, such as drilling, milling, and trimming.

Acknowledgments The work reported herein is sponsored by the National Natural Science Foundation of China (51305352) and "the Fundamental Research Funds for the Central Universities" China (3102014JCS05008).

References

1. Che D, Saxena I, Han P et al (2014) Machining of carbon fiber reinforced plastics/polymers: a literature review. J Manuf Sci Eng 136(3):034001
2. Liu DF, Tang YJ, Cong WL (2012) A review of mechanical drilling for composite laminates. Compos Struct 94(4):1265–1279
3. Palanikumar K, Latha B, Senthilkumar VS et al (2012) Analysis on drilling of glass fiber-reinforced polymer (GFRP) composites using grey relational analysis. Mater Manuf Process 27(3):297–305
4. Kalla D, Sheikh-Ahmad J, Twomey J (2010) Prediction of cutting forces in helical end milling fiber reinforced polymers. Int J Mach Tools Manuf 50(10):882–891
5. Azmi AI, Lin RJT, Bhattacharyya D (2013) Machinability study of glass fibre-reinforced polymer composites during end milling. Int J Adv Manuf Technol 64(1-4):247–261
6. Davim JP, Mata F (2005) Optimisation of surface roughness on turning fibre-reinforced plastics (FRPs) with diamond cutting tools. Int J Adv Manuf Technol 26(4):319–323
7. Işık B (2008) Experimental investigations of surface roughness in orthogonal turning of unidirectional glass-fiber reinforced plastic composites. Int J Adv Manuf Technol 37(1-2):42–48
8. Montoya M, Calamaz M, Gehin D et al (2013) Evaluation of the performance of coated and uncoated carbide tools in drilling thick CFRP/aluminium alloy stacks. Int J Adv Manuf Technol 68(9-12): 2111–2120
9. Wang H, Sun J, Li J et al (2014) Investigation on delamination morphology during drilling composite laminates. Int J Adv Manuf Technol 74(1-4):257–266
10. Silva D, Teixeira JP, Machado CM (2014) Methodology analysis for evaluation of drilling-induced damage in composites. Int J Adv Manuf Technol 71(9-12):1919–1928
11. KoPlev A, Lystrup A, Vorm T (1983) The cutting process, chips, and cutting forces in machining CFRP. Composites 14(4):371–376
12. Wang DH, Ramulu M, Arola D (1995) Orthogonal cutting mechanisms of graphite/epoxy composite. Part I: unidirectional laminate. Int J Mach Tools Manuf 35(12):1623–1638
13. Wang DH, Ramulu M, Arola D (1995) Orthogonal cutting mechanisms of graphite/epoxy composite. Part II: multi-directional laminate. Int J Mach Tools Manuf 35(12):1639–1648
14. Wang X M, Zhang L C (1999) Machining damage in unidirectional fibre-reinforced plastics [C]. Proceedings of the Third International Conference on Abrasive Technology: Current Development and Applications I, Brisbane. 429-436
15. Wang XM, Zhang LC (2003) An experimental investigation into the orthogonal cutting of unidirectional fibre reinforced plastics. Int J Mach Tools Manuf 43(10):1015–1022
16. Arola D, Ramulu M (1997) Orthogonal cutting of fiber-reinforced composites: a finite element analysis. Int J Mech Sci 39(5):597–613
17. Arola D, Sultan MB, Ramulu M (2002) Finite element modeling of edge trimming fiber reinforced plastics. J Manuf Sci Eng 124(1): 32–41
18. Rao GVG, Mahajan P, Bhatnagar N (2007) Micro-mechanical modeling of machining of FRP composites—cutting force analysis. Compos Sci Technol 67(3):579–593
19. Rao GVG, Mahajan P, Bhatnagar N (2007) Machining of UD-GFRP composites chip formation mechanism. Compos Sci Technol 67(11):2271–2281
20. Bhatnagar N, Ramakrishnan N, Naik NK et al (1995) On the machining of fiber reinforced plastic (FRP) composite laminates. Int J Mach Tools Manuf 35(5):701–716
21. Pwu HY, Hocheng H (1998) Chip formation model of cutting fiber-reinforced plastics perpendicular to fiber axis. J Manuf Sci Eng 120(1):192–196
22. Zhang L, Zhang H, Wang X (2001) A force prediction model for cutting unidirection fiber-reinforced plastics. Mach Sci Technol 5(3):293–305
23. Jahromi AS, Bahr B (2010) An analytical method for predicting cutting forces in orthogonal machining of unidirectional composites. Compos Sci Technol 70(16):2290–2297
24. Xu YL, Reifsnider KL (1993) Micromechanical modeling of composite compressive strength. J Compos Mater 27(6):572–588
25. Reifsnider K L, Case S W (2002) Damage tolerance and durability of material systems. pp. 435. ISBN 0-471-15299-4. Wiley-VCH, April 2002., 1
26. Vizzini AJ, Lagace PA (1987) The buckling of a delaminated sublaminate on an elastic foundation. J Compos Mater 21(12): 1106–1117
27. Qi Z, Zhang K, Cheng H, et al. (2015) Microscopic mechanism based force prediction in orthogonal cutting of unidirectional CFRP. Int J Adv Manuf Technol, 1-11

28. Hobbiebrunken T, Fiedler B, Hojo M et al (2005) Microscopic yielding of CF/epoxy composites and the effect on the formation of thermal residual stresses. Compos Sci Technol 65(10):1626–1635
29. Piispanen V (1948) Theory of formation of metal chips. J Appl Phys 19(10):876–881
30. Winkler E (1867) Die lehre yon der elastizitat und festigkeit. Prague: H Dominicus 141:182–184
31. DOI O, YOKOYAMA M (1975) Cutting force analysis of wood: 1st report. Orthogonal cutting accompanied with split ahead of tool. Bull JSME 18(122):905–912
32. Li H, Qin X, He G, et al. (2015) Investigation of chip formation and fracture toughness in orthogonal cutting of UD-CFRP. Int J Adv Manuf Technol. 1-10
33. Padgett WJ, Durham SD, Mason AM (1995) Weibull analysis of the strength of carbon fibers using linear and power law models for the length effect. J Compos Mater 29(14):1873–1884